HHS Public Access

Author manuscript

Biomaterials. Author manuscript; available in PMC 2019 July 01.

Published in final edited form as:

Biomaterials. 2018 July ; 170: 82–94. doi:10.1016/j.biomaterials.2018.03.052.

Src Activation Decouples Cell Division Orientation from Cell Geometry in Mammalian Cells

Xiaoyan Sun[1,2,3,4], **Hongsheng Qi**[5], **Xiuzhen Zhang**[1,2,3], **Li Li**[1,2,3,6], **Jiaping Zhang**[1,2,3], **Qunli Zeng**[1,2,3], **George S. Laszlo**[7], **Bo Wei**[8], **Tianhong Li**[9], **Jianxin Jiang**[10], **Alex Mogilner**[11], **Xiaobing Fu**[4], and **Min Zhao**[1,2,3]

[1]Institute for Regenerative Cures, University of California, Davis, California, USA

[2]Department of Dermatology, University of California, Davis, California, USA

[3]Department of Ophthalmology, University of California, Davis, California, USA

[4]Wound Healing and Cell Biology Laboratory, Institute of Basic Medical Science, Trauma Center of Postgraduate Medical School, Chinese PLA General Hospital, 28 Fu Xing Road, Beijing 100853, P. R. China

[5]Key Laboratory of Systems and Control, Academy of Mathematics and Systems Science, Chinese Academy of Sciences, No. 55 Zhongguancun East Road, Beijing 100190, P. R. China

[6]Department of Respiratory Disease, Daping Hospital, Third Military Medical University, Chongqing 400042, P. R. China

[7]Clinical Research Division, Fred Hutchinson Cancer Research Center, 1100 Fairview Ave, Seattle, USA

[8]Department of General Surgery, Chinese PLA General Hospital, 28 Fu Xing Road, Beijing 100853, P. R. China

[9]Division of Hematology/Oncology, University of California Davis Comprehensive Cancer Center, 4501 X St #3016, Sacramento, USA

[*]**Corresponding author:** Min Zhao, Institute for Regenerative Cures, University of California at Davis CA, School of Medicine, 2921 Stockton Blvd., Room 1617, Sacramento, CA 95817. Tel. 916 7039381; Fax: 916 7039384; minzhao@ucdavis.edu, or Xiaobing Fu, Wound Healing and Cell Biology Laboratory, Institute of Basic Medical Science, Trauma Center of Postgraduate Medical School, Chinese PLA General Hospital, 28 Fu Xing Road, Beijing 100853. Tel. 0086-10-66936345; Fax: 0086-10-66936345; fuxiaobing@vip.sina.com.

Conflict of Interest: The authors state no conflict of interest.

Author contributions

X.Y.S., A.M., X.B.F. and M.Z. conceived ideas and designed the experiments.
X.Y.S., X.Z.Z., L.L., J.P.Z. and Q.L.Z. performed the experiments and analyzed the results.
B.W., T.L., G. S. L. and J.X.J. provided materials.
X.Y.S., A.M. and M.Z. wrote the manuscript.
H. S. Q. and A. M. constructed the mathematical model

Competing financial interests

The authors declare no competing financial interests

[10]State Key Laboratory of Trauma, Burns, and Combined Injury Research, Institute of Surgery, Daping Hospital, Third Military Medical University, Chongqing 400042, China

[11]Courant Institute, Department of Biology, New York University, 251 Mercer St, New York, USA

Abstract

Orientation of cell division plane plays a crucial role in morphogenesis and regeneration. Misoriented cell division underlies many important diseases, such as cancer. Studies with Drosophila and C. elegance models show that Src, a proto-oncogene tyrosine-protein kinase, is a critical regulator of this aspect of mitosis. However, the role for Src in controlling cell division orientation in mammalian cells is not well understood. Using genetic and pharmacological approaches and two extracellular signals to orient cell division, we demonstrated a critical role for Src. Either knockout or pharmacological inhibition of Src would retain the fidelity of cell division orientation with the long-axis orientation of mother cells. Conversely, re-expression of Src would decouple cell division orientation from the pre-division orientation of the long axis of mother cells. Cell division orientation in human breast and gastric cancer tissues showed that the Src activation level correlated with the degree of mitotic spindle misorientation relative to the apical surface. Examination of proteins associated with cortical actin revealed that Src activation regulated the accumulation and local density of adhesion proteins on the sites of cell-matrix attachment. By analyzing division patterns in the cells with or without Src activation and through use of a mathematical model, we further support our findings and provide evidence for a previously unknown role for Src in regulating cell division orientation in relation to the pre-division geometry of mother cells, which may contribute to the misoriented cell division.

Keywords

Cell division orientation; Src; cell geometry; mitosis; cell polarity

1. Introduction

Properly oriented cell division contributes to cell fate choice, tissue architecture, and morphogenesis. A cell's attachment to its adhesive microenvironment controls cell division axis through an intracellular signaling network in animals [1–3]. In asymmetric cell division, a conserved framework whereby cells asymmetrically distribute polarity-related molecules at the cell cortex controls the positioning of the mitotic spindle, and subsequently, cell division orientation. The partitioning defective (Par) complex, consisting of Par3, Par6 and atypical protein kinase C (aPKC), functions as a master polarity determinant involved in generation and maintenance of cortical polarity [4, 5].

Cell geometry, particularly the long axis of non-spherical cells, also determines the orientation of division. In sea urchin embryos, when an applied mechanical force triggers a cell shape alteration, the cells tend to divide along their long axis (so called "long axis rule") [6, 7]. In plants, when cells divide in regions experiencing mechanical conflicts due to differential growth or spatial constraint, they build a new cell wall in the direction of maximal tension, irrespective of cell shape [8]. The evidence that mechanical cues might be

involved in orienting the mitotic spindle also came from a series of experiments using single cells grown on adhesive micropatterns with defined geometry [9, 10]. In these experiments, the author indicated that the pattern of the extracellular matrix (ECM) could override the effect of cell geometry and dictate the axis of cell division [9].

Misoriented cell division and alterations in cell polarity proteins are common in a wide variety of cancers [11, 12]. As the first oncogene discovered, Src is an important signaling intermediate in multiple oncogenic signaling pathways and its overexpression and/or high levels of activation occur frequently in tumor tissues [13]. However, inhibition of Src would result in loss of cortical cues and lead to spindle orientation defects [9]. Early observations also indicated an involvement of Src in the positive regulation of proper cell division orientation [14, 15]. Given these findings, it is likely that the roles of Src in modulating cell division orientation are conflicting: Src is abnormally activated in cancer cells, which have been linked to misoriented cell divisions; whereas inhibition of Src appears to be responsible for the decreased cell division orientation in living cells [9, 14, 15].

Src in humans is encoded by the Src gene. The Src-family tyrosine kinases (SFKs) is comprised of nine family members: c-Src, Yes, Fyn, lyn, lck, Hck, Fgr, Blk, and Yrk that share similar structure and function [16, 17]. The structure of c-Src protein is composed of seven parts [13, 17, 18]: a myristoylated N-terminal segment (SH4 domain), a unique domain, followed by SH3, SH2, linker and tyrosine kinase domains (SH1 domain), and a short C-terminal negative regulatory region. The activity of the Src kinases is regulated through dephosphorylation/phosphorylation of specific tyrosine residues (Tyr416 and Tyr527). Src family tyrosine kinases play a crucial role in the assembly of focal adhesions, migration and invasion [19, 20]. Src affects cell adhesion and migration mainly through interactions with integrins [21], actins [22], GTPase-activating proteins [23], scaffold proteins, such as $p130^{CAS}$ and paxillin [21], and kinases such as focal adhesion kinases (FAKs) [24, 25]. Src can also interact physically with multiple tyrosine kinase receptors via its SH2 domain and activate a cascade of downstream targets as well as modification of the cooperating receptor [13, 19]. These receptors include EGFR, ErbB2, PDGFR, FGFR, CSF1R, VEGFR and Met (hepatocyte growth factor receptor) [26–33].

In the present study, we used genetic and pharmacological approaches to determine the role of Src in the geometry and adhesion pattern-regulated cell division orientation. We employed both micro-contact printing and electric fields (EFs) to control cell geometry and orientation of the long axis of cells, and demonstrated that Src decouples cell geometry from cell division orientation. We also showed that Src affects cell division orientation in breast and gastric cancer cells. Meanwhile, we propose a mechanism underlying the role of Src in guiding cell division orientation by examining the distribution of cortical actin-related proteins in the cells with or without Src activation. By analyzing the division patterns and aided by a mathematical model, we validated the plausibility of our hypothesis that Src activation regulates the accumulation and local density of adhesion proteins to the sites of cell-matrix attachment to affect the force balance on the spindle pole, which subsequently induces cell division misorientation.

2. Experimental procedures

2.1 Cell culture and division on micro-pattern

Wild type mouse embryonic fibroblast (WT-MEF), SYF (*src, yes*, and *fyn* triple knockout), SYF-KD (kinase-inactive Src), and c-Src (SYF knockdown and mouse *c-src* re-expressed) cell lines were gifts from Dr. George S. Laszlo and Prof. Jonathan A. Cooper (Clinical Research Division, Fred Hutchinson Cancer Research Center, Seattle, USA.). The expression of total Src and pY416-Src (p-Src) was verified by Western blotting (Fig. 1L). WT-MEF, SYF, c-Src and SYF-KD cells and mammary cancer cell line MCF-7 cells were cultured in DMEM with 10% FCS and 2 mM glutamine at 37°C, and seeded on micropattern printed glass coverslips (CYTOOChips, CYTOO) in a 6-well plate according to the manufacturer's instructions. Briefly, cells were pelleted, resuspended in DMEM with 30% FCS and plated at 60,000 cells per well. As soon as cells began to attach, the culture medium was changed and the coverslip surface gently flushed to remove all unattached cells. Wells were incubated at 37°C for 2h to allow full cell spreading. The culture media was replaced with CO_2-independent medium (Gibco) containing 30% FCS and cell division was recorded overnight via time-lapsed phase contrast microscopy at 37°C.

2.2 Inhibitor treatments

PP2 (10μM, Calbiochem) was added to culture medium 2 hours after cell spreading on micropatterns and incubated overnight.

2.3 EF stimulation

Electric fields are known to polarize and orient cell division. EFs were applied to cells *in vitro* via an electric chamber, as described previously [34] : A roof consisting of a No. 1 glass coverslip was sealed on top of 2 smaller coverslips spaced 10mm apart with high vacuum silicone grease (Corning) in a 100mm culture dish (Falcon). The final interior dimension of the chamber, through which the electric current was passed, was 20 mm ×10 mm × 0.2 mm. WT-MEF, SYF-KD and c-Src cells were seeded at 1×10^4 cells/cm^2 in electric chambers on Falcon tissue culture dishes for 3h, allowing them to settle and adhere to the base of the dish, before EF exposure. Different strengths of EFs (100, 200 or 300 mV/mm) were supplied from a DC power source connected to silver/silver chloride electrodes immersed in Steinberg's solution and current was passed across the electric chamber through agar–salt bridges anchored at opposite ends of the chamber. This prevented diffusion of electrode products into the cultures. Cultures were recorded as outlined below.

2.4 Video microscopy

We used an inverted microscope (Axiovert 200, Zeiss) with a heated and motorized stage combined with a six-well plate to hold the printed glass coverslip. Metamorph software (Universal Imaging) was used for image acquisition. Hundreds of divisions were recorded overnight using time-lapse phase-contrast microscopy on a multi-field acquisition at a frame rate of one picture every 5 min with a 10x objective. MATLAB 7.0 software was used to measure the angular distribution of spindle orientations. The distribution of division orientation was analyzed as described previously [35] with minor modifications to give a

mean orientation index (OI) of ($\Sigma n \cos[2(90-\theta)]/n$), where θ is the angle between the long axis of cell division and the horizontal direction of the pattern geometry. In EFs, θ is defined as the angle between the long axis of cell division and the EF vector.

2.5 Tissue preparation

Collection of breast cancer patient tissue samples from surgical resections, in total four cancer samples and two normal samples, was approved by the institutional review board of the University of California at Davis. Four gastric cancer tissues and matching normal tissues were obtained from the General Hospital of PLA with the informed consent of patients and institutional approval. A hematoxylin and eosin–stained section of all specimens from each patient was evaluated by a board-certified pathologist (GZ) for diagnosis confirmation and tumor content.

2.6 Sample preparation and staining

Interphase cells on micropatterned coverslips were fixed in 4% paraformaldehyde for 30 min and permeabilized in 0.2% Triton X-100 in PBS for 10 min. Paraformaldehyde-fixed tissue was rinsed in PBS, then permeabilized. The following primary antibodies were used in combination with appropriate Alexa-Fluor-conjugated secondary antibodies (1:200, Invitrogen): rabbit polyclonal PAR-3 (1:500, 07-330 Millipore); Alexa-Fluor-488 conjugated anti phosphorylated Src on Tyr 416 (1:200, 16-248 Millipore); mouse monoclonal Vinculin (1:200, ab18058 Abcam); rabbit polyclonal pericentrin (1:4000, ab4448 Abcam); mouse monoclonal E-Cadherin (1:100, 14472 Cell Signaling); DNA was stained using DAPI (H-1200 Vector Labs). A recommended ICC/IF protocol was used for the detection of pericentrin (http://www.abcam.com/Pericentrin-antibody-ab4448-protocols.html).

2.7 Western blot

The expression of Src in WT-MEF, SYF, SYF-KD, c-Src, MCF-7 and PP2 treated MCF-7 cells was verified by Western blotting. The following primary antibodies were used: rabbit anti-phospho-Src (Try416) (1:1000, 2101 Cell Signaling), rabbit anti-Src (1:1000, 2108 Cell Signaling), and mouse anti-GAPDH (1:3000, G8795 Sigma–Aldrich) was used as an internal control. HRP-conjugated antibody (1:2000, Invitrogen) was used as a secondary antibody.

2.8 In vivo cell division orientation measurements

In vivo cell division orientation was measured with 3-dimensional reconstructions of serial stacks, showing dividing cells at different angles of rotation and unambiguously identify the position of centrosomes. Imaging was carried out with an Olympus FluoView FV1000 confocal microscope. Stacks were collected at 0.25 μm intervals and were imported into Image J 1.46e for analysis. Cell division angle relative to the apical surface of the breast ductal epithelium or gastric mucus was calculated from the spindle axis vector and a vector running tangential to the apical surface of the epithelium (Fig. 3G, I). To confirm accuracy of calculations, measurements were also performed visually in the same images by three independent scorers in a blind fashion and the results were averaged.

2.9 Statistical Analysis

The uniformity of angular data was assessed by conducting the Rao's Spacing Test, and the threshold for statistical significance was set at $p<0.05$. Meanwhile, the results were also subjected to statistical analysis with SPSS v16.0 software for evaluation of directionality. P values were calculated with non-parametric two-tailed Kolmogorov-Smirnov test.

3. Results

3.1 Cell geometry regulated cell division orientation

We first used micropatterned substratum to control cell geometry. Wild type mouse embryonic fibroblast (WT-MEF) cells were plated on four different fibronectin coated patterns. Cells on a disc-shape (Fig. S1B) or crossbow (Fig. S1C) micropattern showed random distribution of division orientations, similar to cells on a non-patterned culture dish (Fig. S1A). When grown on "I"-type or "Y"-type micropatterns, cells elongated and oriented their division axis along the underlying pattern (50% of dividing cells showed division direction between 54 to 126 degrees; Fig. S1D, E). We used the "I"-type micropattern in the following experiments for easy definition of the orientation of long axis of cells. During mitosis, cells on "I"-type micropattern first rounded up, then elongated to reach their final length before becoming furrowed, and divided into two daughter cells.

3.2 Src decoupled cell division orientation from cell geometry on a micropatterned substratum

To determine the role of Src activation in cell division orientation, we used serial strains of genetically modified cell lines, or acute pharmacological inhibition. We plated SYF cells (*src, yes*, and *fyn* triple knockout) on the "I"-type micropattern. The cell division axis of SYF cells was oriented preferentially parallel to the long axis of the "I"-type micropattern with a significantly higher percentage of cells dividing in an angle between 54 to 126 degree (62%; Fig. 1A, B), when compared with that in WT-MEFs ($p<0.01$, Fig. 1A, B, D). Re-expression of Src (c-Src cells) abolished the increase and the c-Src cells divided with a cell division orientation the same as that in WT-MEFs (Fig. 1A, B). The gain of function (more oriented cell division in SYF cells) and loss of function (less oriented cell division in c-Src cells) suggest strongly that Src activation decouples cell division orientation from long axis orientation of mother cells.

We then tested if Src kinase activity was responsible for the decoupling effect. We used SYF cells re-expressing a kinase-inactive Src mutant (SYF-KD). SYF-KD cells on the "I"-type micropattern showed an enhanced cell division orientation preferentially parallel to the long axis of the adhesive pattern (60% in an angle range from 54 to 126 degree; Fig. 1A, B). We next tested whether treatment of WT-MEFs with the Src inhibitor PP2 could recapitulate the results observed in SYF cells. PP2 treatment induced cell division orientation preferentially parallel to the long axis of the "I"-type micropattern (62% in an angle range of 54 to 126 degree; Fig. 1A, B). Therefore, inhibition of Src kinase activity contributed to cell division orientation associated with the long axis of the micropatterns (Fig. 1D; Movie S1).

3.3 Src decoupled cell division orientation from long axis of cells aligned in an electric field

To test the above results in a different model of controlled orientation of cell long axis, we used electric fields (EFs). When cultured in an EF, MEF cells elongated and oriented their long axis perpendicular to the field line of an applied EF (Fig. 1H–J; Fig. S2). Exposure to an EF did not induce the orientation of cell division in WT-MEFs, which showed randomized orientation similar to the control cells without EF administration (Fig. 1E, H). when the Src kinase-inactive SYF-KD cells were exposed to the EFs, however, these cells showed significantly oriented cell division along the long axis of mother cells ($p<0.01$, Fig. 1F, I). Src re-expression abolished the oriented cell division (Fig. 1G, J). Inhibition of Src using PP2 resulted in increased cell division orientation perpendicular to applied EFs (Fig. S3A–3C). The same effect of PP2 in orienting cell divisions perpendicular to the field line was confirmed with a human skin fibroblast cell line (BJ cells, ATCC) (Fig. S3D–3H).

Collectively, these data suggest that Src activation decouples cell division orientation from the long axis of the mother cells aligned either by adhesion pattern or by applied electric fields.

3.4 Src inhibition contributed to the correct orientation of mitotic cancer cells

Aberrant activation of Src is found in many types of cancers, including lung, breast, pancreatic, colon, and prostate cancers [36–39]. To investigate the roles of *c-src* in regulating cell division orientation in cancer cells, we plated MCF-7 breast cancer cells on the “I”-type micropattern. MCF-7 cells plated on an “I”-type micropattern showed random cell division orientation (Fig. 2A). PP2 treatment led to the reorientation of mitotic MCF-7 cells along the long axis of the “I”-type micropattern (62% in an angle range of 54 to 126 degree; Fig. 2B, D).

3.5 Src upregulation correlated with cell division misorientation in cancer

To further investigate the role of Src in cell division orientation in cancers, we used confocal microscopy to determine the cell division orientation in breast and gastric cancer tissues. Orientation of mitotic cells was determined in three 3-dimensional reconstructions of serial stacks in the cancerous or noncancerous tissues stained with DNA dyes and antibodies that recognize centrosomes (Fig. 3G, I). Only mitotic cells that met the following criteria were used for analysis [40]: the displacement of a condensed mitotic nucleus toward the apical surface with the presence of two pericentrin-positive spots, which tend to be brighter in mitosis and in different positions than in nonmitotic cells (Fig. 3E, F; arrow). The expression of Par-3 was used to determine the apical surface in breast ductal epithelium (Fig. 3A, B). We observed that the expression patterns of Par-3 were different between cancerous and normal breast tissues, which correlated significantly with the expression of phosphorylated Src (p-Src). In cancerous tissue, the expression of Par-3 was co-localized with the expression of p-Src and distributed at the apical surface of breast ductal epithelial cells (Fig. 3A; Fig. S4A–4C). In normal tissues, Par-3 expression revealed a more regular spaced arrangement, and was co-localized with p-Src expression at the apical-lateral surface of breast ductal epithelial cells (Fig. 3B; Fig. S4D–4F). Three-dimensional analysis revealed differences between cell division orientation in cancerous and normal tissues. In normal tissues, the

mitotic cells tended to orient their division axes horizontally to the apical surface of ductal epithelium (52.05% 0°–30°, 22.99% 30°–60°, 24.96% 60°–90°, respectively, Fig. 3H). In cancer tissues, however, the preferred horizontal mitotic alignment was lost in p-Src-expressing cells, and significantly fewer cells were observed to divide horizontally along the apical surface in cancerous breast ductal epithelial cells (34.6% 0°– 30°, 33.35%30°–60°, 32.05% 60°–90°, respectively, Fig. 3H) when compared with those in normal cells.

We also examined the Src-induced cell division misorientation in human gastric tumor tissues. Par-3 had similar distribution patterns in normal breast and gastric tissue samples (Fig. 3D), and was co-localized with p-Src in gastric cancerous cells (Fig. 3C). Given that Par-3 exhibited aberrant polarity in the cytoplasm of gastric cancer cells (Fig. 3C), the expression of E-cadherin was then used to determine the apical surface in both normal and cancerous gastric epithelial cells (Fig. 3F). Consistent with our previous findings, the orientation of cell division was aligned parallel to the apical surface of normal gastric epithelial cells (47.27% 0°–30°, 24.55% 30°–60°, 28.18% 60°–90°, respectively, Fig. 3J). Overexpression of Src, however, reduced the percentage of mitotic cells with horizontal alignment and induced the cell division misorientation in gastric cancer tissues (37.5% 0°–30°, 34.52% 30°–60°, 27.98% 60°–90°, respectively, Fig. 3J).

3.6 Src controlled the distribution of cortical cues

To determine the mechanism by which Src activation decoupled cell division orientation from the long axis of mother cells, we investigated Par-3, in part due to its co-localization with p-Src in breast and gastric cancer tissues. In SYF cells, Par-3 was expressed uniformly in the cytoplasm after plating on “I”-type micropattern, (Fig. 4A, D). When the Src level was high, Par-3 was recruited to the sites of cell-matrix adhesion, normally at corners of the cells (Fig. S5). Par-3 distributed differently at the adhesive sites in c-Src over-expressing cells on “I”-type micropattern. 42.3% of cells showed fluorescent distribution of Par-3 in four-corner attachment, 25.6% in three-corner attachment, 14.1% in two-corner attachment, and 2.6% in one-corner attachment (Fig. 4G–J). Vinculin was chosen as another protein associated with cortical actin activity [41]. In SYF cells, vinculin was distributed homogeneously at the sites of cell attachment to ECM (in almost all SYF cells, Fig. 4B, E). Src re-expression, however, caused a differential distribution of vinculin to the sites of cell-matrix adhesion (45.5% in four-corner attachment, 21.8% in three-corner attachment, 20% in two-corner attachment, and 12.7% in one-corner attachment; Fig. 4K–N).

As a member of the ERM protein family, ezrin serves as an intermediate between the plasma membrane and the actin cytoskeleton [42], and plays a key role in organizing polarity in mitotic cells [9]. We detected the expression of phosphorylated ezrin (p-ezrin) on the cell cortex in both SYF and c-Src overexpressing cells. In SYF cells, the patches of p-ezrin expression were preferentially localized at the sites of cell-matrix attachment (260/298, 87.2%, Fig. 4C, F). In c-Src-overexpressing cells, however, the expression of p-ezrin was consolidated to form bright patches that showed diverse distribution at the sites of cell-matrix attachment (54.5% in four-corner attachment, 24.8% in three-corner attachment, 14.9% in two-corner attachment, and 3.3% in one-corner attachment; Fig. 4O–R). These results demonstrated that Src overexpression contributed to the consolidated and

heterogeneous distribution of cortical cue-related proteins at the sites of cell-matrix adhesion.

3.7 Src regulated cell-adhesive patterns in guiding cell division orientation

The adhesive environment of a cell is known to exert mechanical forces on the cell [7]. Cell shape, in turn, is a manifestation of these adhesive and tensional patterns [43]. Studies in both single cells and tissues have indicated that mechanical force induced by an adhesive pattern is an important cue for cell division orientation during mitosis [7]. To test the role of Src in regulating adhesion-related force balance in spindle pole which eventually led to the misorientation of cell division, we initially picked up mitotic divisions with cell-matrix attachment on all of the four corners in SYF, SYF-KD and PP2-treated WT-MEF cells after plating on the “I”-type micropattern. When the cells attached uniformly to the four adhesive corners, these cells contracted equally to finally form a cubic shape before rounding up (Fig. 5A, B). The distribution of cell division axes in SYF, SYF-KD and PP2-treated WT-MEF cells were oriented parallel to the long axis of the adhesive micropattern (64% in SYF, 61% in SYF-KD and 63% in PP2-treated WT-MEF cells; Fig. 5D). We picked the similar mitotic division cells with four-corner attachment in WT-MEF and c-Src overexpressing cells. Strikingly, the distribution of cell division axes in WT-MEF and c-Src overexpressing cells were also oriented and aligned parallel to the long axis of the “I”-type micropattern (65% in WT-MEF, 61% in c-Src; Fig. 5D). Moreover, we analyzed the mitotic divisions with three- and two- corner attachment on the sites of cell-matrix adhesion after plating on “I”-type micropattern in SYF, SYF-KD, PP2-treated, WT-MEF and c-Src overexpressing cells (Fig. S6). Imbalanced cell contraction owing to uneven cell contact with its underlying adhesive substrate led to changes in cell shape. The mitotic cells ultimately formed triangular, horizontal spindle and opposite spindle shape in response to the asymmetric contraction before their rounding up. In most cases, the cells oriented their division axes parallel to the long axis of generated adhesive sites (Fig. S6A–D). However, when combining all the above divisions with differential cell-matrix adhesive patterns (four- corner, three- and two- corner attachment) together, the orientation of mitotic cells in SYF, SYF-KD and PP2-treated WT-MEF cells were still oriented parallel to the long axis of the underlying micropattern (62% in SYF, 60% in SYF-KD and 62% in PP2-treated WT-MEF cells; Fig. 5E). Cell division in WT-MEF and c-Src overexpressing cells tended to be less oriented (50% in WT-MEF, 49% in c-Src cells; Fig. 5E), owing to a lower percentage of four-corner attachment patterns in these cells (65.6% in WT-MEF and 67.2% in c-Src overexpressing cells) than in the Src kinase-inhibited cells (82.2% in SYF, 81.3% in SYF-KD and 85.4% in PP2-treated WT-MEF cells, respectively; Fig. S7 and Movie S2).

Additionally, to further address the role of adhesive patterns on cell division orientation, we plated SYF cells on the medium size I-type micropattern to break the balanced four-corner adhesion pattern and induce localized deprivation of cell-matrix attachment on the cell cortex (Movie S3). The medium size micropattern is bigger than that (small size micropattern) used in our experimental system. SYF cells on the medium size micropattern shifted their attachment on the cell-matrix adhesion frequently. Cell division on medium size micropattern became significantly less oriented when compared with those on smaller size micropattern ($p<0.05$, Fig. 5F). Only 49% of the cells oriented their division along the long

axis of adhesive micropattern (angle range from 54 to 126 degree; Fig. 5F). Our results confirmed the contributions of adhesive patterns to cell division orientation, and supported the hypothesis that Src regulated cell-adhesive patterns in guiding cell division orientation (Fig. 5G).

3.8 Computational analysis of Src-induced cell division orientation

A mathematical model has previously been derived to describe the relationship of mitotic cell orientation and the distribution of cortex cues [10]. Here, we used this model to test our quantitative understanding of the role of Src activation. We used a simple plane geometric representation of the spindle following [10], not counting spindle distortion and microtubule bending (Fig. 6A; Fig. S8A–8D). The simplifying assumption is that the cell is a circle with radius R, and the spindle is characterized by two poles with the distance $2a$ between them. The cell orientation is denoted by the angle $\phi([-\pi/2, \pi/2])$ between the x-axis and the spindle axis (Fig. 6A). The cortical angle of each point on the cell cortex is denoted by ψ ($\in [0, 2\pi]$), and the spindle-cortex vector is $\vec{R}(\psi) = [\cos\ \psi, \sin\ \psi]^T$.

The cortical force applied to the spindle in the tangential direction by the astral microtubules is given by

$$\vec{f}(\psi, \phi) = F(\psi)\rho(\psi - \phi)\vec{\mathrm{m}}(\psi, \phi)$$

where F(ψ) denotes the magnitude of force applied to each microtubule at the cortical angle ψ, and it is proportional to the following dimensionless quantity

$$g(\psi) = \frac{1}{R}\sqrt{\left(\frac{\mathrm{d}x}{\mathrm{d}\psi}\right)^2 + \left(\frac{\mathrm{d}y}{\mathrm{d}\psi}\right)^2}$$

which is relative to the parameterized positions ($x(\psi)$, $y(\psi)$) = ($R\cos\ \psi + v_x(\psi)$, $R\sin\ \psi + v_y(\psi)$), with their variation $v(\psi)$ = ($v_x(\psi)$, $v_y(\psi)$) measured from the pattern center. Taking into account measured data for the spindle center's position distribution (Fig. 6B), the proper degree polynomials were found to approximate function $v(\psi)$ = ($v_x(\psi)$, $v_y(\psi)$). Thus we have

$$F(\psi) = C_1 g(\psi)$$

where C_1 is a constant coefficient.

In the expression for the force, $\rho(\theta)$ is the angular density of microtubules that accesses the cell cortex at angle θ, that is:

$$\rho(\theta) = \frac{N(\psi)}{2\pi}\frac{\mathrm{d}\alpha}{\mathrm{d}\theta}$$

where $N(\psi)$ denotes the total number of microtubules emerging from one spindle pole. Since the I-type micropattern was used in our experiments, and we assume that the force generators are distributed uniformly throughout the adhesion pattern, $N(\psi)$ has the form:

$$N(\psi) = \begin{cases} C_2, \frac{1}{4}\pi \le \psi \le \frac{3}{4}\pi \text{ or } -\frac{3}{4}\pi \le \psi \le -\frac{1}{4}\pi \\ 0, \text{ otherwise} \end{cases}$$

where C_2 is a constant parameter.

Using trigonometric formulas (Fig. 6A), $\alpha(\theta)$ can be calculated from the following expression:

$$\alpha(\theta) = \begin{cases} \pi - \arccos\left(\frac{a - R\cos\theta}{\sqrt{a^2 + R^2 - 2aR\cos\theta}}\right), \phi \le \psi \le \phi + \pi \\ \arccos\left(\frac{a - R\cos\theta}{\sqrt{a^2 + R^2 - 2aR\cos\theta}}\right) - \pi, \phi - \pi \le \psi < \phi \end{cases}$$

In the expression for the force, $\vec{m}(\psi, \phi)$ is a unit vector as $[\cos \gamma(\psi, \phi), \sin \gamma(\psi, \phi)]^T$ with $\gamma = \alpha(\theta) + \phi$.

Therefore, a net torque exerted by the force generators is:

$$\tau(\phi) = \int_{-\pi}^{\pi} \vec{R} \times \vec{f}\, d\psi = \int_{-\pi}^{\pi} (R_x f_y - R_y f_x) d\psi$$

Following [10], the effective energy landscape is defined as

$$W(\phi) = -\int_{-\pi/2}^{\phi} \tau_z(\phi') d\phi'$$

The minima of $W(\phi)$ corresponds to the stable cell division orientations. The orientation of the cell division in our system was studied experimentally on a small size “I”-type micropattern, where the center positions (Fig. 6B–D) and angular distributions (Fig. 6F–H) of the dividing cells during mitosis were measured. We used the model to calculate and plot the potential energy landscape $W(\phi)$ for the uniform force generator distribution in the “I”-type micropattern (Fig. 6E’). Then, we computed the potential energy landscape from the observed cell orientation distributions in the three cases shown in Fig. 6F–H (Fig. 6F’–H’). The theoretical energy profiles for the cells without Src activation (SYF-KD, WT-PP2) fitted from the experimentally measured angular distribution histograms (Fig. 6F’, G’) were very close to the idealized energy profile (Fig. 6E’), indicating that in these cells the distribution of the cortex force generators were uniform. On the other hand, the energy profile in c-Src overexpressing cells (Fig. 6H’) found from the observed cell division orientation distribution (Fig. 6H) was different, indicating that Src contributed to the heterogeneous distribution of

the adhesive molecules at the sites of cell-matrix attachment. In fact, in cells with Src activation, the distribution of cell adhesion molecules correlated with the localization of the cell-matrix attachment. Also, the cell center during division shifted away from the pattern center (Fig. 6D).

4. Discussion

The determination of cell division orientation and spindle apparatus orientation during mitosis is largely dependent on cell shape, long axis orientation, and the geometry of the adhesive microenvironment [9, 43]. Proper orientation control is critical to morphogenesis, tissue regeneration, and homeostasis. Therefore, dysfunctions in orientation control is associated with dysfunctional cell growth, i.e. cancer. It is well known that abnormal Src activation is involved in many types of cancers. However, the conventional wisdom is that Src activation maintains the fidelity between cell division orientation and cell shape and adhesion pattern. This work suggests an unrecognized role for Src in misoriented cell division – namely, activation of Src plays a significant role in decoupling cell division orientation from the orientation of the long axis of mother cells. In this study, we used two different external cues to orient the long axes of cells – adhesion pattern and electric fields. Both have robustly oriented the long axes of cells. Using SYF *src* knockout cell line for ablation of Src signaling caused a gain of function in MEF cells. Significantly, more cells divided following the long axis of their mother cells. Re-expression of *src* caused loss of function – less oriented cell division following the long axis of mother cells. Using Src kinase-inactive cells (SYF-KD), we demonstrated that it is a kinase-dependent process. This result is supported by pharmacological inhibition of Src in several cell types, including breast cancer cells. These data provide strong evidence suggesting Src activation's contribution to misoriented cell division, perhaps in cancer. In addition, the immunofluorescence detection of Par-3, vinculin and ezrin indicated that Src affected the distribution of cortical cues on cell cortex to manipulate the accumulation and local density of adhesive proteins to the sites of cell-matrix attachment. By analyzing differential division patterns in the cells with or without Src expression and using a mathematical model, we further presented a corroborating and quantitative understanding of our hypothesis that Src regulated cell-adhesive patterns in guiding cell division orientation.

Moreover, our previous study and the research by others showed that cultured cells could respond to direct-current EFs and elongate perpendicularly to the EF vector [44–46]. An emerging theory suggests that the cells tend to elongate and align their cytoskeletal major axis perpendicular to the force direction to minimize the EF gradient [45]. In consistence with previous findings, the SYF-KD cell aligned its long axis perpendicular to the EF and showed a higher aspect ratio (length-to-width) during mitosis when compared with WT-MEF cells (Fig. S9A). Re-expression of Src, however, united the diversity in cell shape and size, showing a corresponding lower length-to-width ratio (Fig. S9A). Our hypothesis is consistent with these phenomena, supported by the finding that Src contributes to heterogeneous accumulation of adhesion proteins to the sites of cell attachment to ECM. This may in turn lead to differences in the sensitivity to exogenous EFs and may account for the fact that Src inhibits the EF-induced cell elongation (Fig. S9B).

Cells in situ, within organs or tissues, are embedded in a highly structured microenvironment, i.e. the extracellular matrix (ECM) and neighboring cells [47]. The topology of the microenvironment imposes specific physical and mechanical cues that influence the spatial distribution of adhesion molecules at sites of cell-matrix and cell-cell contacts (Fig. S4D–4F) [7, 8, 48]. Accumulating data in the literature indicates that the orientation of cell division in mammalian cells is dominated by cell adhesion and the associated retraction fibers developed in the interphase [7, 9, 43]. These retraction fibers exert tensile forces and transmit extracellular signals about the adhesive pattern to the mitotic cell through a series of mechano-sensing mechanisms [7, 43, 49]. As the most-studied mechano-sensory complexes, the cell adhesion molecule not only provides a mechanical link between the actomyosin cytoskeleton and the ECM, but also serves as the protein sensor through which signal transduction occurs in response to external mechanical cues [49]. However, the interactions between cells and their ECM are dynamic and reciprocal [49]. Transcellular tension transmitted across adherens junctions affects ECM remodeling, which in turn directs the localization of cell– matrix and cell–cell adhesions, and further modulates the lipid membrane composition, actin dynamics (e.g. protrusion and contraction), microtubule stability and eventually the polarity of the entire cell [7, 43, 49]. The ECM topological reorganization and alterations in spatio-mechanical cues are also important for cell division orientation and morphogenesis [8, 48]. Given these findings, the cell-matrix and cell-cell adhesions and related proteins in mechano-sensing and mechano-transduction play critical roles in various cellular activities, including motility, morphological changes, proliferation, differentiation and cortical polarity formation. Although studies conducted in recent years have provided insight into the mechanisms concerning adhesion-mediated mechano-sensing and mechano-transduction, there is also a need to elucidate the intrinsic biomolecules and their involvement in regulation of the cortical organization of cell adhesion molecules that correlate with the activities of subcortical actin filaments. The global, interwoven regulation of cellular response to these extrinsic (applied) and/or intrinsic (cell-generated) cues will contribute to our better understanding on ordered behavior of cell populations, tissue morphogenesis, and pathogenesis of many human diseases, including the development of cancer. Here, we demonstrated genetically and pharmacologically, in two experimental models, a novel role of Src: Src activation resulted in the localized deprivation or accumulation of cell adhesions at sites of cell-matrix and cell-cell contacts. This subsequently affected the assembly of actin filaments in response to the geometry of external adhesive conditions and led to the dysregulation of cell division orientation during mitosis. Our data indicated Src as an intrinsic factor that modulates the distribution of cortical signals during mitotic division. This novel effect also highlights the importance of this oncogene in tumorogenesis in addition to the other known functions of Src activation in cell proliferation [50] and migration [51]. Particularly, we found that the expression of Par-3 was irregular in breast and gastric cancerous epithelial cells when compared to the corresponding normal controls (Fig. 3A, C; Fig. S4). Unusual activation of Src and aberrant changes in Par-3 distribution resulted in a decrease in the lateral cell-to-cell association in both breast and gastric cancerous tissues (Fig. 3A, C; Fig. S4), which may represent one of the mechanical and biochemical basis responsible for the uncontrolled growth and invading activity of cancer cells.

In conclusion, Src regulated the accumulation and local density of adhesive proteins to the sites of cell-matrix attachment. Src activation renders fewer adhesion sites, which may affect the mechanical force balance on the spindle pole and subsequently induce cell division misorientation. This novel role of Src suggests another important aspect of Src in tumorigenesis and metastasis where misoriented cell division and uncontrolled migration are keys to malignancy.

Supplementary Material

Refer to Web version on PubMed Central for supplementary material.

Acknowledgments

We thank prof. Jonathan A. Cooper for providing Src genetically-modified cell lines and their information. The work is supported by grants from NIH (1R01EY019101), California Institute of Regenerative Medicine (RB1-01417), NSF (MCB-0951199), and Research to Prevent Blindness, Inc. Research in the Author's lab is also supported by NSFC (30901564, 81101883, 81372067, 81230041, 81121004, 81421064), National Basic Science and Development Programme (973 Programme, 2012CB518105), Beijing Novel Program (2008B53, 2009A38).

References

1. Lechler T, Fuchs E. Asymmetric cell divisions promote stratification and differentiation of mammalian skin. Nature. 2005; 437(7056):275–80. [PubMed: 16094321]
2. Lu B, Roegiers F, Jan LY, Jan YN. Adherens junctions inhibit asymmetric division in the Drosophila epithelium. Nature. 2001; 409(6819):522–5. [PubMed: 11206549]
3. Fernandez-Minan A, Martin-Bermudo MD, Gonzalez-Reyes A. Integrin signaling regulates spindle orientation in Drosophila to preserve the follicular-epithelium monolayer. Current biology : CB. 2007; 17(8):683–8. [PubMed: 17363255]
4. Knoblich JA. Mechanisms of asymmetric stem cell division. Cell. 2008; 132(4):583–97. [PubMed: 18295577]
5. Siller KH, Doe CQ. Spindle orientation during asymmetric cell division. Nature cell biology. 2009; 11(4):365–74. [PubMed: 19337318]
6. Minc N, Piel M. Predicting division plane position and orientation. Trends in cell biology. 2012; 22(4):193–200. [PubMed: 22321291]
7. Nestor-Bergmann A, Goddard G, Woolner S. Force and the spindle: mechanical cues in mitotic spindle orientation. Semin Cell Dev Biol. 2014; 34:133–9. [PubMed: 25080021]
8. Louveaux M, Julien JD, Mirabet V, Boudaoud A, Hamant O. Cell division plane orientation based on tensile stress in Arabidopsis thaliana. Proc Natl Acad Sci U S A. 2016; 113(30):E4294–303. [PubMed: 27436908]
9. Thery M, Racine V, Pepin A, Piel M, Chen Y, Sibarita JB, Bornens M. The extracellular matrix guides the orientation of the cell division axis. Nat Cell Biol. 2005; 7(10):947–53. [PubMed: 16179950]
10. Thery M, Jimenez-Dalmaroni A, Racine V, Bornens M, Julicher F. Experimental and theoretical study of mitotic spindle orientation. Nature. 2007; 447(7143):493–6. [PubMed: 17495931]
11. Pease JC, Tirnauer JS. Mitotic spindle misorientation in cancer--out of alignment and into the fire. Journal of cell science. 2011; 124(Pt 7):1007–16. [PubMed: 21402874]
12. Noatynska A, Gotta M, Meraldi P. Mitotic spindle (DIS) orientation and DISease: cause or consequence? The Journal of cell biology. 2012; 199(7):1025–35. [PubMed: 23266953]
13. Kim LC, Song L, Haura EB. Src kinases as therapeutic targets for cancer. Nature reviews. Clinical oncology. 2009; 6(10):587–95.
14. Bei Y, Hogan J, Berkowitz LA, Soto M, Rocheleau CE, Pang KM, Collins J, Mello CC. SRC-1 and Wnt signaling act together to specify endoderm and to control cleavage orientation in early C. elegans embryos. Developmental cell. 2002; 3(1):113–25. [PubMed: 12110172]

15. Nakayama Y, Matsui Y, Takeda Y, Okamoto M, Abe K, Fukumoto Y, Yamaguchi N. c-Src but not Fyn promotes proper spindle orientation in early prometaphase. The Journal of biological chemistry. 2012; 287(30):24905–15. [PubMed: 22689581]
16. Martin GS. The hunting of the Src. Nature reviews. Molecular cell biology. 2001; 2(6):467–75. [PubMed: 11389470]
17. Yeatman TJ. A renaissance for SRC. Nature reviews. Cancer. 2004; 4(6):470–80. [PubMed: 15170449]
18. Mezquita B, Mezquita P, Pau M, Mezquita J, Mezquita C. Unlocking Doors without Keys: Activation of Src by Truncated C-terminal Intracellular Receptor Tyrosine Kinases Lacking Tyrosine Kinase Activity. Cells. 2014; 3(1):92–111. [PubMed: 24709904]
19. Wu JC, Chen YC, Kuo CT, Wenshin Yu H, Chen YQ, Chiou A, Kuo JC. Focal adhesion kinase-dependent focal adhesion recruitment of SH2 domains directs SRC into focal adhesions to regulate cell adhesion and migration. Sci Rep. 2015; 5:18476. [PubMed: 26681405]
20. Schoenherr C, Serrels B, Proby C, Cunningham DL, Findlay JE, Baillie GS, Heath JK, Frame MC. Eps8 controls Src- and FAK-dependent phenotypes in squamous carcinoma cells. J Cell Sci. 2014; 127(Pt 24):5303–16. [PubMed: 25359883]
21. Playford MP, Schaller MD. The interplay between Src and integrins in normal and tumor biology. Oncogene. 2004; 23(48):7928–46. [PubMed: 15489911]
22. Zhang Z, Lin SY, Neel BG, Haimovich B. Phosphorylated alpha-actinin and protein-tyrosine phosphatase 1B coregulate the disassembly of the focal adhesion kinase × Src complex and promote cell migration. The Journal of biological chemistry. 2006; 281(3):1746–54. [PubMed: 16291744]
23. Brown MT, Andrade J, Radhakrishna H, Donaldson JG, Cooper JA, Randazzo PA. ASAP1, a phospholipid-dependent arf GTPase-activating protein that associates with and is phosphorylated by Src. Molecular and cellular biology. 1998; 18(12):7038–51. [PubMed: 9819391]
24. Westhoff MA, Serrels B, Fincham VJ, Frame MC, Carragher NO. SRC-mediated phosphorylation of focal adhesion kinase couples actin and adhesion dynamics to survival signaling. Molecular and cellular biology. 2004; 24(18):8113–33. [PubMed: 15340073]
25. Mitra SK, Hanson DA, Schlaepfer DD. Focal adhesion kinase: in command and control of cell motility. Nature reviews. Molecular cell biology. 2005; 6(1):56–68. [PubMed: 15688067]
26. Tice DA, Biscardi JS, Nickles AL, Parsons SJ. Mechanism of biological synergy between cellular Src and epidermal growth factor receptor. Proceedings of the National Academy of Sciences of the United States of America. 1999; 96(4):1415–20. [PubMed: 9990038]
27. Muthuswamy SK, Siegel PM, Dankort DL, Webster MA, Muller WJ. Mammary tumors expressing the neu proto-oncogene possess elevated c-Src tyrosine kinase activity. Molecular and cellular biology. 1994; 14(1):735–43. [PubMed: 7903421]
28. Bowman T, Broome MA, Sinibaldi D, Wharton W, Pledger WJ, Sedivy JM, Irby R, Yeatman T, Courtneidge SA, Jove R. Stat3-mediated Myc expression is required for Src transformation and PDGF-induced mitogenesis. Proceedings of the National Academy of Sciences of the United States of America. 2001; 98(13):7319–24. [PubMed: 11404481]
29. Landgren E, Blume-Jensen P, Courtneidge SA, Claesson-Welsh L. Fibroblast growth factor receptor-1 regulation of Src family kinases. Oncogene. 1995; 10(10):2027–35. [PubMed: 7761103]
30. Courtneidge SA, Dhand R, Pilat D, Twamley GM, Waterfield MD, Roussel MF. Activation of Src family kinases by colony stimulating factor-1, and their association with its receptor. The EMBO journal. 1993; 12(3):943–50. [PubMed: 7681396]
31. Wrobel CN, Debnath J, Lin E, Beausoleil S, Roussel MF, Brugge JS. Autocrine CSF-1R activation promotes Src-dependent disruption of mammary epithelial architecture. The Journal of cell biology. 2004; 165(2):263–73. [PubMed: 15117969]
32. Mukhopadhyay D, Tsiokas L, Zhou XM, Foster D, Brugge JS, Sukhatme VP. Hypoxic induction of human vascular endothelial growth factor expression through c-Src activation. Nature. 1995; 375(6532):577–81. [PubMed: 7540725]
33. Empereur S, Djelloul S, Di Gioia Y, Bruyneel E, Mareel M, Van Hengel J, Van Roy F, Comoglio P, Courtneidge S, Paraskeva C, Chastre E, Gespach C. Progression of familial adenomatous

polyposis (FAP) colonic cells after transfer of the src or polyoma middle T oncogenes: cooperation between src and HGF/Met in invasion. British journal of cancer. 1997; 75(2):241–50. [PubMed: 9010033]

34. Zhao M, Song B, Pu J, Wada T, Reid B, Tai G, Wang F, Guo A, Walczysko P, Gu Y, Sasaki T, Suzuki A, Forrester JV, Bourne HR, Devreotes PN, McCaig CD, Penninger JM. Electrical signals control wound healing through phosphatidylinositol-3-OH kinase-gamma and PTEN. Nature. 2006; 442(7101):457–60. [PubMed: 16871217]
35. Song B, Zhao M, Forrester JV, McCaig CD. Electrical cues regulate the orientation and frequency of cell division and the rate of wound healing in vivo. Proceedings of the National Academy of Sciences of the United States of America. 2002; 99(21):13577–82. [PubMed: 12368473]
36. Irby RB, Yeatman TJ. Role of Src expression and activation in human cancer. Oncogene. 2000; 19(49):5636–42. [PubMed: 11114744]
37. Corey SJ, Anderson SM. Src-related protein tyrosine kinases in hematopoiesis. Blood. 1999; 93(1): 1–14. [PubMed: 9864140]
38. Finn RS. Targeting Src in breast cancer. Annals of oncology : official journal of the European Society for Medical Oncology/ESMO. 2008; 19(8):1379–86.
39. Giaccone G, Zucali PA. Src as a potential therapeutic target in non-small-cell lung cancer. Annals of oncology : official journal of the European Society for Medical Oncology/ESMO. 2008; 19(7): 1219–23.
40. Quyn AJ, Appleton PL, Carey FA, Steele RJ, Barker N, Clevers H, Ridgway RA, Sansom OJ, Nathke IS. Spindle orientation bias in gut epithelial stem cell compartments is lost in precancerous tissue. Cell stem cell. 2010; 6(2):175–81. [PubMed: 20144789]
41. Yonemura S, Wada Y, Watanabe T, Nagafuchi A, Shibata M. alpha-Catenin as a tension transducer that induces adherens junction development. Nature cell biology. 2010; 12(6):533–42. [PubMed: 20453849]
42. Casaletto JB, Saotome I, Curto M, McClatchey AI. Ezrin-mediated apical integrity is required for intestinal homeostasis. Proceedings of the National Academy of Sciences of the United States of America. 2011; 108(29):11924–9. [PubMed: 21730140]
43. Thery M, Bornens M. Cell shape and cell division. Curr Opin Cell Biol. 2006; 18(6):648–57. [PubMed: 17046223]
44. Bai H, McCaig CD, Forrester JV, Zhao M. DC electric fields induce distinct preangiogenic responses in microvascular and macrovascular cells. Arterioscler Thromb Vasc Biol. 2004; 24(7): 1234–9. [PubMed: 15130919]
45. Zhang J, Ren R, Luo X, Fan P, Liu X, Liang S, Ma L, Yu P, Bai H. A small physiological electric field mediated responses of extravillous trophoblasts derived from HTR8/SVneo cells: involvement of activation of focal adhesion kinase signaling. PLoS One. 2014; 9(3):e92252. [PubMed: 24643246]
46. Tandon N, Goh B, Marsano A, Chao PH, Montouri-Sorrentino C, Gimble J, Vunjak-Novakovic G. Alignment and elongation of human adipose-derived stem cells in response to direct-current electrical stimulation. Conf Proc IEEE Eng Med Biol Soc. 2009; 2009:6517–21. [PubMed: 19964171]
47. Thery M. Micropatterning as a tool to decipher cell morphogenesis and functions. Journal of cell science. 2010; 123(Pt 24):4201–13. [PubMed: 21123618]
48. Galletti R, Verger S, Hamant O, Ingram GC. Developing a 'thick skin': a paradoxical role for mechanical tension in maintaining epidermal integrity? Development. 2016; 143(18):3249–58. [PubMed: 27624830]
49. DuFort CC, Paszek MJ, Weaver VM. Balancing forces: architectural control of mechanotransduction. Nat Rev Mol Cell Biol. 2011; 12(5):308–19. [PubMed: 21508987]
50. Beristain AG, Molyneux SD, Joshi PA, Pomroy NC, Di Grappa MA, Chang MC, Kirschner LS, Prive GG, Pujana MA, Khokha R. PKA signaling drives mammary tumorigenesis through Src. Oncogene. 2015; 34(9):1160–73. [PubMed: 24662820]
51. Ishigaki T, Imanaka-Yoshida K, Shimojo N, Matsushima S, Taki W, Yoshida T. Tenascin-C enhances crosstalk signaling of integrin alphavbeta3/PDGFR-beta complex by SRC recruitment

promoting PDGF-induced proliferation and migration in smooth muscle cells. Journal of cellular physiology. 2011; 226(10):2617–24. [PubMed: 21792920]

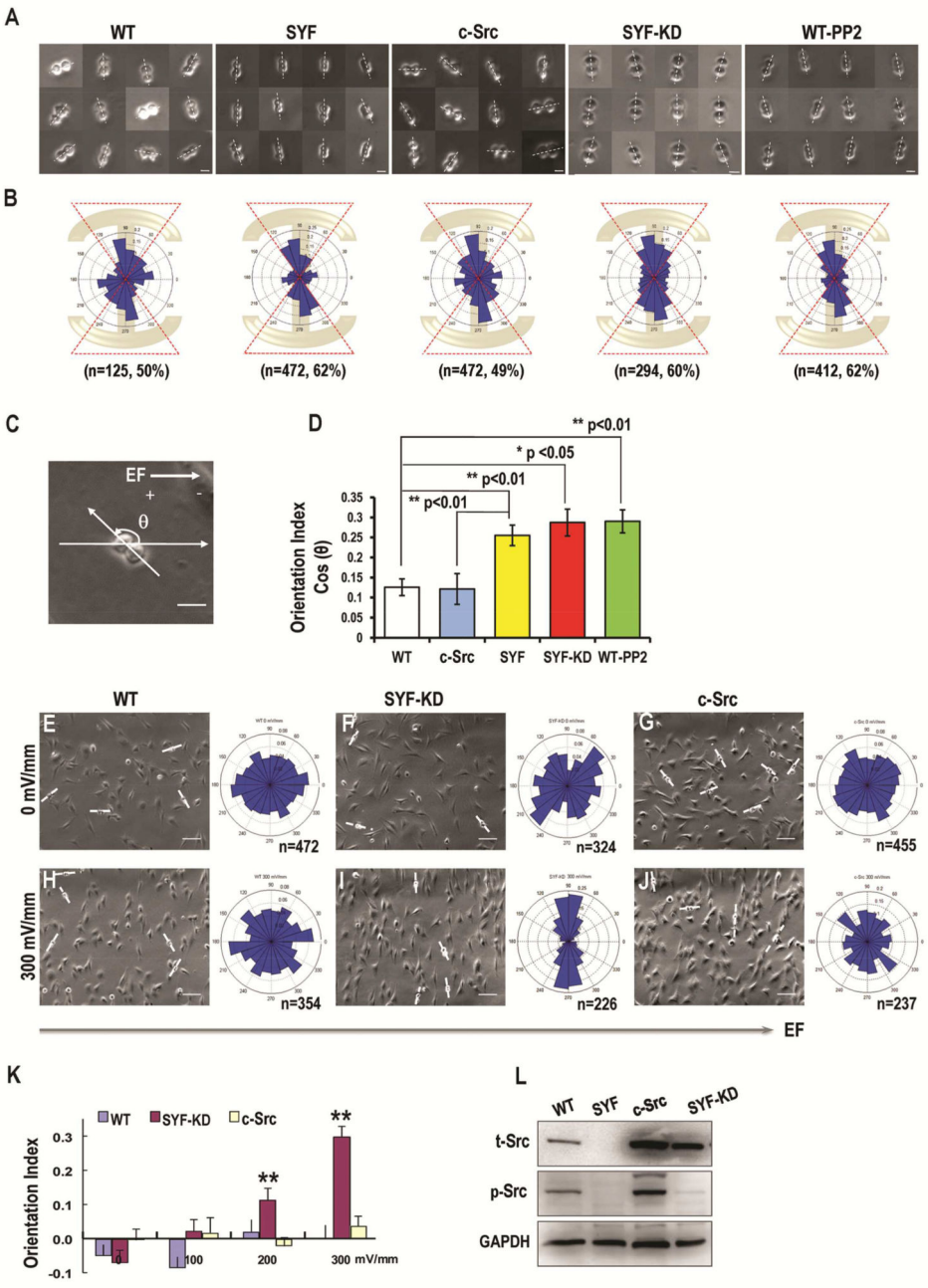

Figure 1. Src knockout significantly increases alignment of cell division orientation in response to extracellular cues

(A) The upper row shows the cell division direction of the WT-MEF (WT), SYF, c-Src, SYF-KD and PP2- treated WT-MEF (WT-PP2) cells after being plated on “I”-type micropattern.

(B) The lower row shows angular distribution of cell division orientations in WT-MEF, SYF, c-Src, SYF-KD and PP2- treated WT-MEF cells.

(C) Schematic to illustrate how angles were defined in EFs. The distribution of division orientation was analyzed by Rayleigh’s distribution to give a mean orientation index of

(Σncos[2(90−θ)]/n). In EFs, the angle between the direction of the longest axis of cell division and that of applied EFs was defined as "θ".

(D) Quantification of cell division orientation index. Cell division was significantly more oriented in response to micropattern in SYF, SYF-KD, and PP2- treated WT-MEF cells.

(E–J). Cell division orientation in an applied EF. SYF-KD cells oriented significantly better in an applied EF than WT cells. Re-expression of Src abolished EF-induced cell division orientation. The right column in e-j shows the angular distribution of cell division orientations in WT-MEF (E, H), SYF-KD (F, I), and Src over-expressing cells (G, J) after exposure to EFs. EFs guided cell division orientation in SYF-KD cells in an EF strength-dependent way (K). These data indicated that Src knockout and re-expression of kinase-inactive Src mutants resulted in significant division orientation of MEF cells in an applied electric field.

(L) The expression of total Src and phosphorylated Src in WT-MEF and different mutant cell lineages were presented in Fig. L. Scale bars represent 20 μm in a, c, and 100 μm in E–J. Results represent mean ± S.D., *P<0.05, **P <0.01. All results are representative of 3 independent experiments.

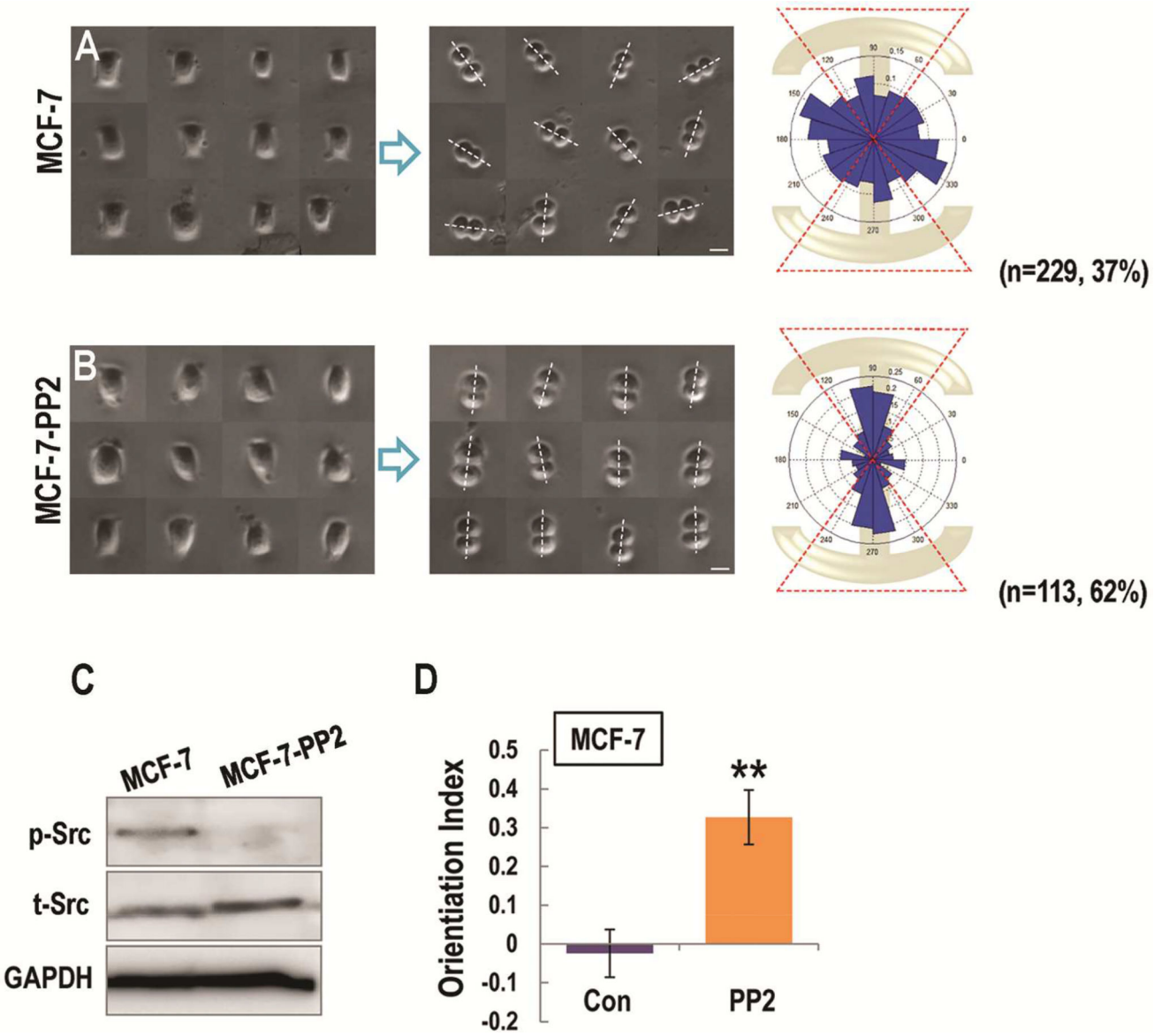

Figure 2. Src inhibition contributed to the correct orientation of mitotic cancer cells *in vitro*

(A, B) Left column shows the interphase of MCF-7 (A, MCF-7), and PP2- treated MCF-7 cells (B, MCF-7-PP2) constrained on the I-type micropattern. The middle column shows the division directions in MCF-7 (A), and PP2- treated MCF-7 cells (B) after plated on I-type micropattern. The right column shows angular distribution of division orientations in MCF-7 (A), and PP2-treated MCF-7 (B) cells.

(C) The expression of total Src and phosphorylated Src in MCF-7 and PP2- treated MCF-7 cells were presented in Fig. C.

(D) Src inhibition significantly contributed to the response of cell division orientation to the geometry of micropatterns in cancerous cells. Scale bars represent 20 μm. Results represent mean ± S.D. **P <0.01 All results are representative of 3 independent experiments.

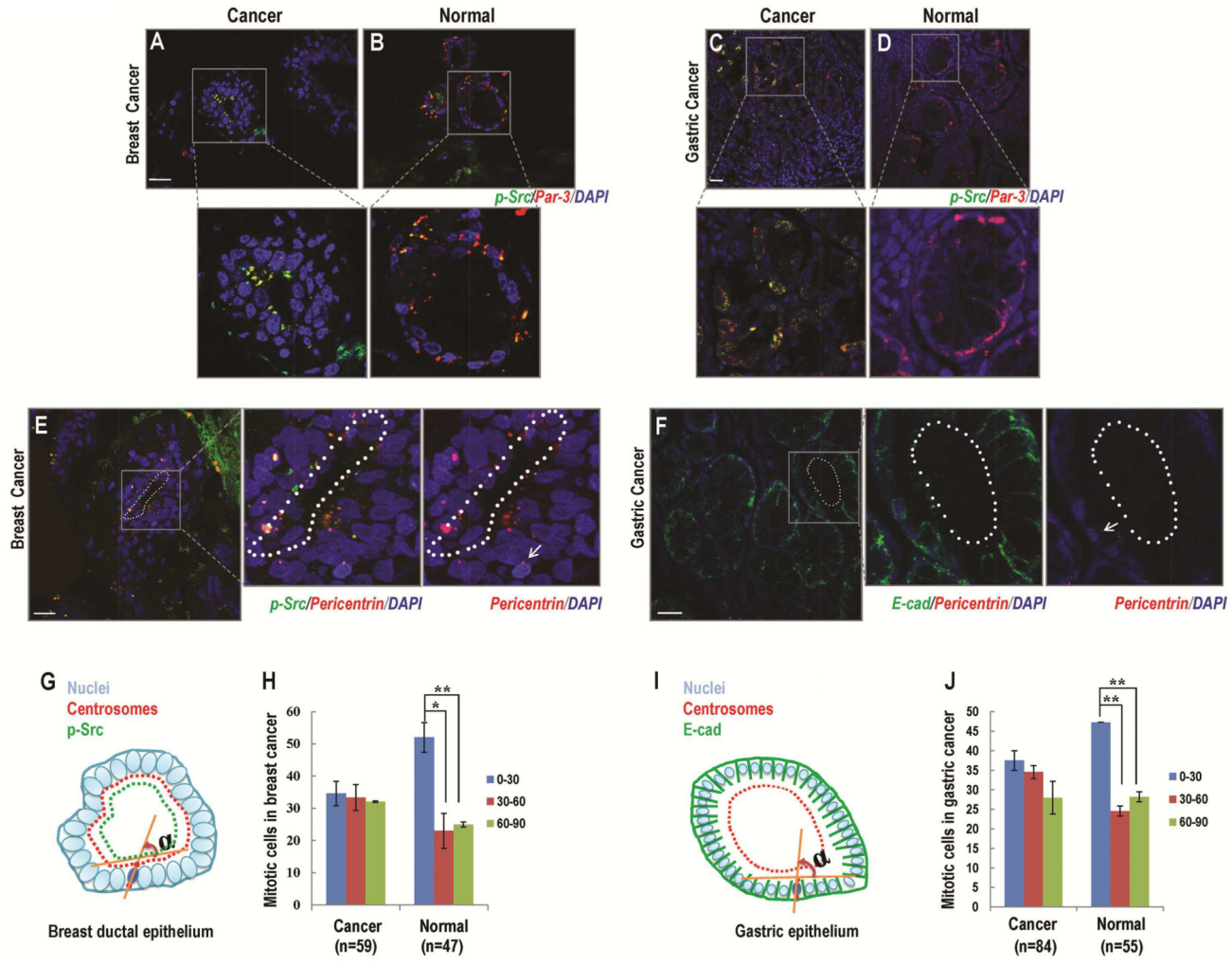

Figure 3. Src upregulation resulted in cell division misorientation in cancer cells *in vivo*

(A, B) Three-dimensional reconstruction of Par-3 staining in breast cancerous tissue (A) and normal breast tissue (B). In cancer tissues, the expression of Par3 (red) was co-localized with the expression of p-Src (green) and distributed at the apical surface of breast ductal epithelial cells (A). In normal tissues, Par-3 expression was co-localized with p-Src expression at the apical-lateral surface of breast ductal epithelial cells (B).

(C, D) Three-dimensional reconstruction of Par-3 staining in gastric cancerous tissue (C) and normal gastric tissue (D). In cancer tissues, Par-3 (red) was observed to co-localize with p-Src (green) in the cytoplasm of gastric cancer cells (C). In normal gastric epithelium, p-Src expression level was low. And, the distribution of Par-3 (red) was detectable at the apical-lateral surface of gastric epithelial cells (D).

(E, F) Three-dimensional reconstruction of p-Src (green, E) and E-cadherin (green, F) staining to visualize the determining of apical surface (dotted lines), centrosomes labeled with pericentrin antibodies (red) to mark spindle poles, and DNA (DAPI, blue) in breast (E) and gastric (F) cancer tissues.

(G, I) Schematic to illustrate the definition of angels. The mitotic orientation was scored as previously described [40]. Briefly, the direction of mitotic cell division was calculated by

using the recorded spatial coordinates of spindle poles (marked by centrosomes; E, F) and the apical surface as a reference point (dotted lines; E, F). The axis that runs tangential to the apical surface of the epithelium where the dividing cell lay was used as the reference axis so that a cell division oriented toward the apical surface of the epithelium at an angle of 0°–30° from this reference line was scored as horizontal. A cell division oriented toward the apical surface at an angle of 60°–90° from this reference line was scored as perpendicular.

(H) The differences between cell division orientation in the cancerous and normal breast tissues.

(J) The differences between cell division orientation in the cancerous and normal gastric tissues. Scale bars represent 20μm. Results represent mean ± S.D. *P <0.05, **P <0.01 All results are representative of 3 independent experiments.

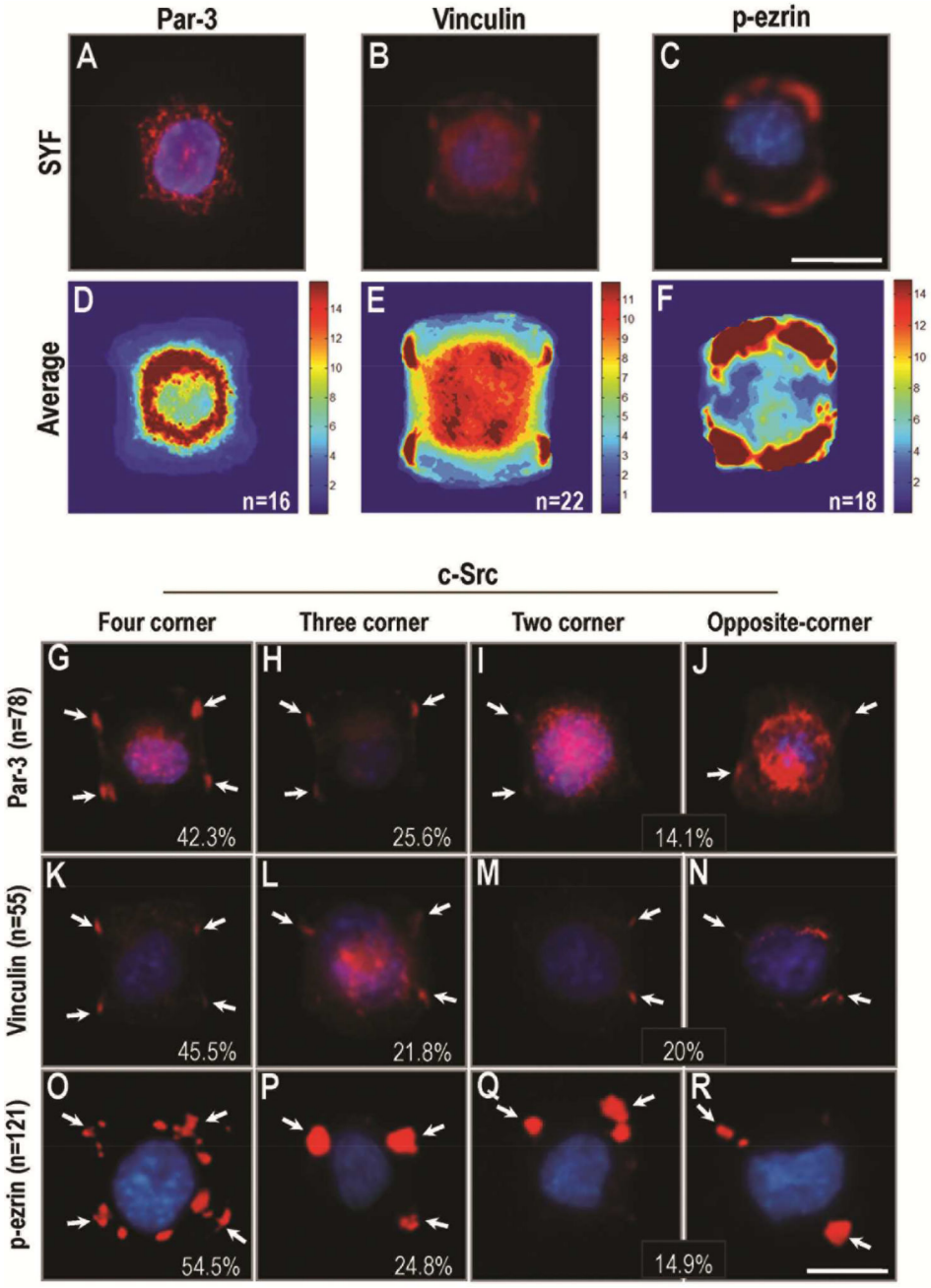

Figure 4. Src controls the distribution of cortical cues on the cell cortex

(A–C) Expression of proteins associated with cortical actin activity in SYF cells after plating on I-type micropattern. Par-3 was expressed uniformly in the cytoplasm of SYF cells (A). Vinculin was distributed at the sites of cell attachment to ECM in almost all SYF cells (B). Expression of p-ezrin was preferentially localized at the sites of cell-matrix attachment in SYF cells (C).

(D–F) The average distribution of Par-3, Vinculin and p-ezrin was shown in D, E, F.

(G–R) Src re-expression contributed to the diverse distribution of Par-3 (G–J), Vinculin (K–N), and p-ezrin (O–R) at the sites of cell-matrix adhesion in c-Src overexpressing cells. (G–

J) The expression of Par-3 in c-Src over-expressing cells after plating on I-type micropattern (42.3% in four-corner attachment, 25.6% in three-corner attachment, and 14.1% in two-corner attachment). (K-N) The expression of Vinculin in c-Src over-expressing cells after plating on I-type micropattern (45.5% in four-corner attachment, 21.8% in three-corner attachment, and 20% in two-corner attachment). (O–R) The expression of ezrin in c-Src over-expressing cells after plating on I-type micropattern (54.5% in four-corner attachment, 24.8% in three-corner attachment, and 14.9% in two-corner attachment). Scale bars represent 20μm. All results are representative of 3 independent experiments.

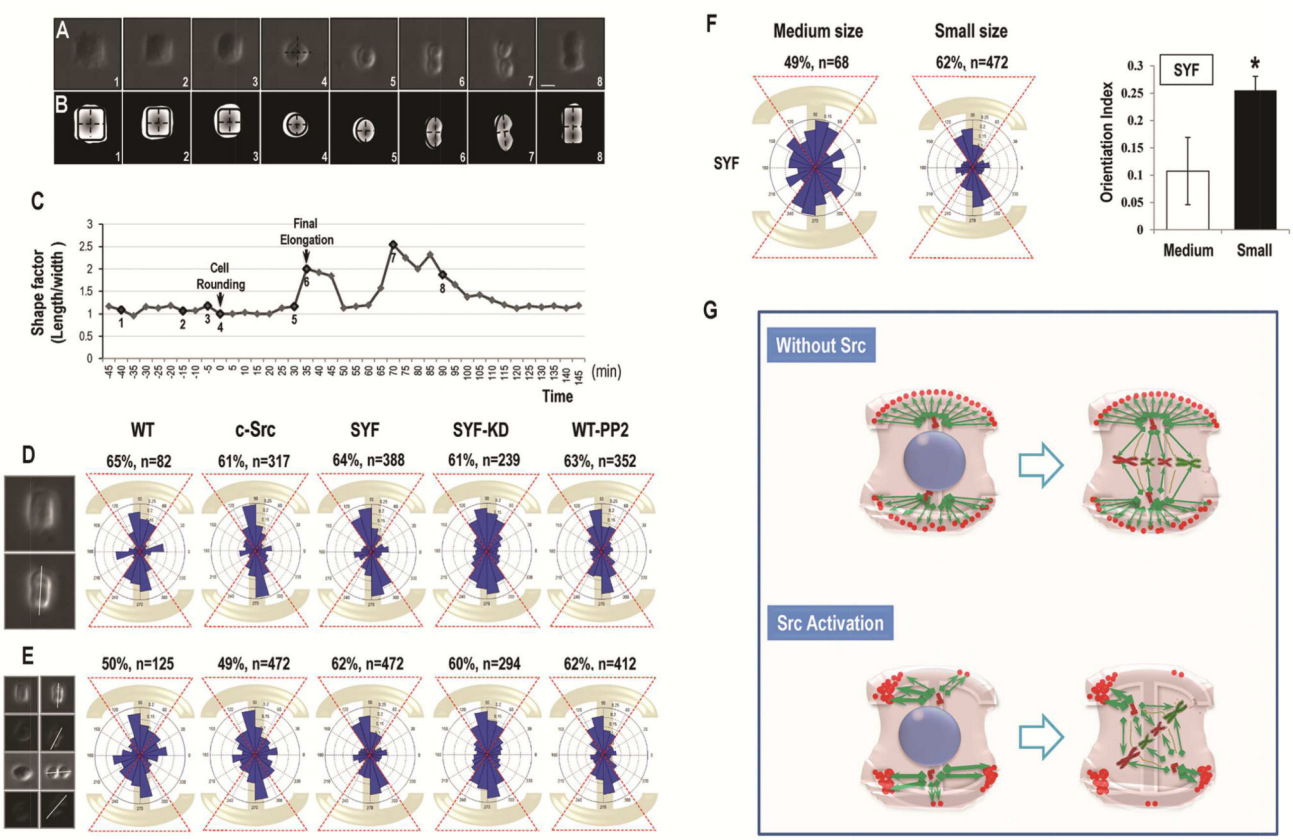

Figure 5. Src controls the accumulation and local density of cell adhesions at the site of cell matrix attachment to manipulate cell division orientation

(A) The mitotic divisions with cell-matrix attachment on all of the four corners in SYF cells. Frames were extracted from a time-lapse phase-contrast microscopy at a rate of one picture every 5 minutes with a 10× objective. Numbers corresponded to those presented on the time curve in C. The mitotic cell center was indicated in frame 4 and the division axis was shown in frame 6.

(B) Canny edge detection to show the changes of center positions in A. Black dashed lines corresponding to the length and width of the mitotic cells were calculated on segmented pictures to show the cell shape factor. The cytoplasm in SYF cells contracted equably and finally formed a cubic shape before rounding up.

(C) Cell shape factor (ratio of length to width) shows the shape changes during mitotic division in SYF cells with four-corner attachment. Time 0 corresponded to the beginning of cell rounding.

(D) The angular distribution of cell division in WT-MEF (WT), c-Src, SYF, SYF-KD, and PP2-treated WT-MEF (WT-PP2) cells with four-corner attachment.

(E) When combining all the cell-division cases (four-corner attachment, three-corner attachment, two-corner attachment, and two opposite-corner attachment) together, the orientation of mitotic divisions in SYF, SYF-KD and PP2-treated WT-MEF cells were still oriented parallel to the long axis of the underlying micropattern, whereas the distribution of cell division axes in WT-MEF and c-Src overexpressing cells tended to be less oriented.

(F) Larger micropatterning induced the localized deprivation of cell-matrix attachment on the cell cortex and broke the balanced four-corner adhesion pattern in SYF cells.
(G) Schematic to show how Src controls the distribution of cell-matrix adhesion on the cell cortex. Without activation of Src, the cortical cue-related protein distributed homogeneously at the sites of cell-matrix adhesion, which aligned the cell division machinery along the longest axis of the cell geometry. Src activation affected the distribution of cortical cues on the cell cortex to manipulate the accumulation and local density of adhesive proteins to the sites of cell-matrix attachment, which ultimately interrupted the force balance on the spindle pole and induced the cell division misorientation. Scale bars represent 20μm. Results represent mean ± S.D. *P <0.05 All results are representative of 3 independent experiments.

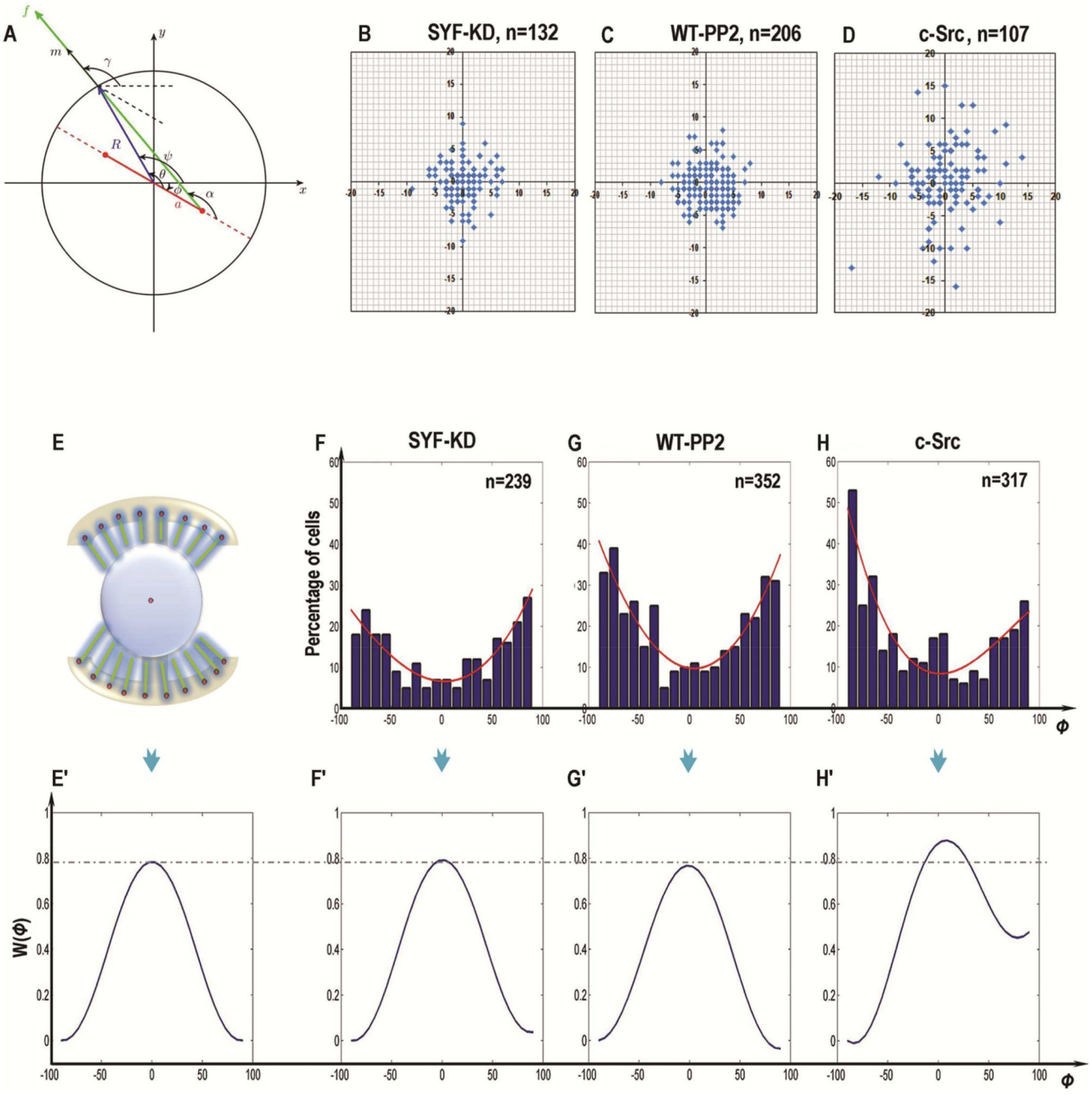

Figure 6. Experimental study of Src-induced cell division orientation

(A) Schematic representation of mitotic spindle geometry for round cells with radius *R*. The spindle poles (red) are separated by distance 2a. The spindle orientation is characterized by angle $\phi(0, \pi/2)$ between the x-axis and the spindle axis. The cortical angle of each pulling force on the cell cortex is denoted by $\psi(\phi, \phi+\pi)$.

(B–D) The center positions of the dividing cells in SYF-KD (B), PP2-treated WT-MEF (C, WT-PP2) and c-Src-overexpressing (D) cells. In the rounding cells, the center positions of SYF-KD and PP2-treated WT-MEF cells were close to the pattern center (B, C). When Src

was activated, however, the cell center during division scattered and changed away from the pattern center (D).

(E, E') The schematic representation to show mitotic cell on I-type micropattern with uniform distribution of adhesive molecules (top, E), and the ideal energy profile $W(\phi)$ theoretically (bottom, E'), where the variation measured from the pattern center is not taken into consideration.

(F–H) Angular distributions of spindle orientation in SYF-KD (F), PP2-treated WT-MEF (G) and c-Src-overexpressing (H) cells were experimentally measured on the "I"-type micropattern during mitosis. The outlines which fit the angular distribution histogram obtained from the experimental data were indicated (red line).

(F'–H') The schematic representations to show the theoretical potential energy landscape $W(\phi)$ in SYF-KD (F'), PP2-treated WT-MEF (G') and c-Src-overexpressing (H') cells.